Science Signaling
AAAS
www.sciencesignaling.org/cgi/content/full/4/176/ra38/DC1

Supplementary Materials for

The cis-Regulatory Logic of Hedgehog Gradient Responses: Key Roles for Gli Binding Affinity, Competition, and Cooperativity

David S. Parker, Michael A. White, Andrea I. Ramos, Barak A. Cohen, Scott Barolo*

*To whom correspondence should be addressed. E-mail: sbarolo@umich.edu

Published 7 June 2011, *Sci. Signal.* **4**, ra38 (2011)
DOI: 10.1126/scisignal.2002077

The PDF file includes:

Section 1. Modeling Different Biophysical Mechanisms

To find models that could account for the *dpp*D-GFP data, we built models of different biophysical mechanisms and attempted to fit these models to the transgenic reporter data. We found that a repressor cooperativity and a differential affinity model fit the data best, qualitatively and quantitatively (Fig. 3, B and C). Here, we explain how we selected repressor cooperativity and differential affinity as the best candidate models to explain the observed expression pattern of *dpp* in the wing disc.

Within our statistical thermodynamic framework, there were four broad categories of models that could be applied to the *dpp*D enhancer: models which allow cooperative interactions between Ci proteins; non-cooperative models; models which assume that Ci_{ACT} and Ci_{REP} exhibit equal affinity for DNA; and differential affinity models which allow Ci_{ACT} and Ci_{REP} to bind DNA with different affinities. In terms of model parameters, non-cooperative models are models in which all three ω parameters representing Ci-Ci interaction energies (table S2) are held fixed at zero, whereas in cooperative models, all three of these parameters are free to take negative (cooperative) or positive (anti-cooperative) values. Cooperative interactions in the model can represent direct cooperative binding, or cooperativity through an unspecified cofactor that makes the binding energy of multiple Ci proteins more than additive.

Equal affinity models contain two Ci-DNA association constants, one of which we fit to the data, whereas the other was chosen to take a biologically reasonable value in order appropriately scale the other model parameters (table S2 and Materials and Methods). Differential affinity models have four different Ci-DNA association constants, one of which is chosen whereas the other three are fit to the data.

We sought to identify models that best fit the data quantitatively and qualitatively. As a quantitative measure of fit, we used the root mean square (RMS) of the residuals, which we calculated by comparing the predicted relative expression (predicted expression minus basal, *dpp*D-Ci^{KO} expression) to the measured relative expression (RFP-normalized, measured expression minus RFP-normalized, basal *dpp*D-Ci^{KO} expression). Qualitatively, we sought models that could accurately predict the regions of repression (relative to basal transcription), activation, and the point in the gradient at which *dpp* expression shifts from activation to repression (identified by circles in figs. S6 and S7).

We fit four different models to the data: equal DNA affinity and cooperative; equal DNA affinity and non-cooperative; differential affinity and cooperative; differential affinity and non-cooperative. The models were fit simultaneously to the 3xCi^{ptc} and 3xCi^{wt} data sets. Quantitatively, the two cooperative models fit the data best (fig. S6, A and B; RMS = 0.044), whereas the two non-cooperative models fit less well (fig. S6, C and D; RMS = 0.057). The non-cooperative equal affinity model (fig. S6C) failed to accurately model the switch from activation to repression under the low-affinity enhancer, one of the most crucial qualitative features of the data, and we therefore eliminated this model from further consideration. The other three models accurately captured the switch from activation to repression in both the low- and high-affinity data, and thus, we considered these models successful both quantitatively and qualitatively.

The fit parameter values of these models suggest the specific biophysical scenarios underlying the models (table S3). In the cooperative models, Ci_{REP}-Ci_{REP} cooperativity and Ci_{ACT}-Ci_{REP} anti-

cooperativity were substantial. In the non-cooperative, differential affinity model, activator exhibited a higher affinity for Ci^{wt} sites than repressor, whereas the reverse was true for high-affinity sites. Thus, our fits to the four general classes of models produced three possible biophysical binding mechanisms that could account for the observed expression of *dpp*: Ci_{ACT}-Ci_{REP} anti-cooperativity, Ci_{REP}-Ci_{REP} cooperativity, and Ci_{ACT} preference for Ci^{wt} sites with Ci_{REP} preference for Ci^{ptc} sites.

Notably, the Ci_{ACT} and Ci_{REP} association constants in the cooperative, differential affinity model were similar (table S3), suggesting that differential affinity contributes little to a cooperative model. Because both cooperative models explain the data equally well quantitatively and qualitatively, we eliminated the cooperative differential affinity model from further consideration and focused on cooperative equal affinity and non-cooperative differential affinity models.

Our initial fit of an equal affinity, cooperative model exhibited strong Ci_{ACT}-Ci_{REP} anti-cooperativity and Ci_{REP}-Ci_{REP} cooperativity (table S3). We next explored whether both of these features were necessary to explain the data by fitting models which included only Ci_{ACT}-Ci_{REP} anti-cooperativity or only Ci_{REP}-Ci_{REP} cooperativity. Our results showed that Ci_{ACT}-Ci_{REP} anti-cooperativity failed to account for the key qualitative features of the data (fig. S7A), whereas Ci_{REP}-Ci_{REP} alone could accurately model *dpp* expression both qualitatively and quantitatively (fig. S7B). Therefore, based on the model fits presented in figs. S6 and S7, we considered repressor cooperativity and non-cooperative differential affinity as the two primary candidate biophysical models that could explain the response of *dpp* to Hedgehog.

Section 2. Parameter Sensitivity Analysis of Repressor Cooperativity and Differential Affinity Models

We explored the robustness of the repressor cooperativity and differential affinity models by examining the effect of changes to individual model parameters. Insensitivity to variation in some parameters suggests that the model's success depends primarily on the biophysical structure underlying the model (*1*), rather than on highly specific parameter values that could be merely a product of the peculiarities of the current data set, our approach to finding the best fit, or the assumptions the model makes about the steepness of the morphogen gradient.

To study model sensitivity to parameter changes, we took the best fit repressor cooperativity or differential affinity model (table S4) and varied individual parameters while holding the other parameters fixed. We measured the effect of parameter changes on the model fit by calculating the RMS as described above.

We varied the steepness of the gradient by changing *D* (fig. S9A; lower *D* produces a steeper gradient). The repressor cooperativity model can tolerate substantial variation in *D* before the quality of the fit degrades. Compared to the repressor cooperativity model, the differential affinity model generally fit best with a steeper gradient (for example, lower values of *D*; compare the x-axis scales for each model in fig. S9A), and the differential affinity model was somewhat more sensitive to changes in *D*. Overall, both models remained largely stable after moderate changes in *D*. This suggests that, particularly for the repressor cooperativity model, the success of these models was not dependent on assumptions we made about the steepness of the Hh gradient.

Both repressor cooperativity and differential affinity models exhibit a stronger sensitivity to changes in total Ci concentration, obtained by varying *h* (fig. S9B). This is due to the effect of *h* on enhancer occupancy (fig. S10). These models are successful when total Ci concentration is such that the weak enhancer is only partially occupied whereas the strong enhancer is nearly saturated. When *h* is too high, both enhancers are fully saturated and the low-affinity enhancer behaves as the high-affinity enhancer. Thus, both repressor cooperativity and differential affinity models predict that the low-affinity, Ci^{wt} enhancer should be unsaturated, whereas the high-affinity Ci^{ptc} enhancer should be saturated.

The most finely tuned parameter in both repressor cooperativity and differential affinity models was the activator-BTC interaction energy ω (fig. S9C; red trace). This contrasted with the repressor-BTC interaction ω (fig. S9C; blue trace), which could take nearly any value without substantially affecting the model fit. Both models work well when the repressor-BTC interaction ω is zero (indicating no interaction between repressor and BTC), which suggests that in these models, the primary effect of repressors is to prevent the binding of activator, and the active inhibition of polymerase binding plays only a small role in the mechanism of repression.

Section 3. Testing Model Fits

We tested the repressor cooperativity and differential affinity models for overfitting by training each model on one enhancer data set and used the resulting parameters to predict the other data set. However, because low-affinity Ci-DNA association constants cannot be fit by training the model to the high-affinity data and vice versa, we held all association constants fixed at the values in table S3. We fit the remaining model parameters to one data set, and used those parameters to predict the other data set.

When trained on only the high-affinity, Ci^{ptc} data, the repressor cooperativity model performed as well as the model fit to all the data (RMS=0.049, compared to RMS=0.048 when fit to both data sets). When trained only on the low-affinity data, the repressor cooperativity model performed less well (RMS=0.054) but still comparable to the best-fit differential affinity model (RMS=0.057). The differential affinity model trained only on the high-affinity data failed to accurately predict the low-affinity data (RMS=0.189). Similarly, when trained only on the low-affinity data, the differential affinity model failed to accurately predict the high-affinity expression pattern (RMS=0.140). These results suggest that the best-fit repressor cooperativity model is naturally consistent with the features both low- and high-affinity data sets, whereas the best-fit DA model can only model both data sets with parameter values that reflect an imperfect compromise between the two data sets.

Methods

In vivo expression constructs

dpp expression constructs were cloned into pH-Stinger (*2*) from which the LacZ reporter cassette was excised with a PstI/SpeI digest. Into this P-element backbone, we cloned a “Flp-out cassette” consisting of two directly repeated FRT sites flanking a nuclear GFP. Three polyadenylation sites were introduced immediately downstream of GFP to minimize transcriptional read-through. We cloned the *dpp* cDNA downstream of the Flp-out cassette. Upstream of the Flp-out cassette, we cloned either the *dppD*-wt or *dppD*-Ciptc enhancer and the *Hsp70* promoter (fig. S4B). In the absence of Flp recombinase, this construct expresses GFP under control of the cloned *dpp*D enhancer (fig. S5, A to C). When Flp recombinase is present and a heat shock is applied, recombination between the FRT sites removes GFP and positions the *Hsp70* promoter immediately upstream of the *dpp* cDNA, allowing expression of *dpp* (fig. S5, D to F; note the loss of GFP signal). In the experiments in figs. S4, C to E, and S5, larvae contain a single copy of Flp recombinase under control of the heat shock promoter (P[*HS-Flp*]) and a single copy of a *dpp* expression construct. Expression of Flp recombinase was induced by a 1-hour 37°C heat shock during the second instar stage.

Figure S1
Annotated sequences of enhancer constructs

A. *ptc* enhancer (827 bp)

-876 to -50 upstream of *ptc* (2R:4,536,264-4,537,090)

```
ATGCATGCGCAGCCTGCCACGCACGCGCTTCCCCCAAACAAATACACACACACACACTGAGACGAAAGCTCCATTG
                                                                      Ci1
GGCAGCGCTGCCGACGCTGAAGGCCGACATCGGCAGAGCTGAACGTTTGGGTAGGGGACCACCCACATCGCTTGGC
                                                  Ci2
GGTTTCAGTTTAATGAAGGCAGAAACAAATTTATTTTTGGGTGGTCCACACTGCAGCGAAAATAAACTACAGTGGC
                                  Ci3
AACAACAAACCAGCAGCCAAGGCACTTTGGGTGGTCCATGCAAAAAAAAAACAAATTACGGCATGCGAATAACAAT
AGAAATTAGCGCTCTCGTGGCGGAGCTATTTGGGTATATTAGAGCTACATATTTTATTTGTTTATAAAAAGTATAA
ATGTAAACAATGAGTTCCAAGCATTAAGTCCGTATGCTCAACAATTACATTATCATTATTATTATCACTTAAATAT
TTACAAAGGATATTTAAACAGTAATAGATATATATTTTATTTCTTAATTTCTGTTAACATATGTATTTACATTGGT
AGTTATTCTTTATTTTGCAACAAGCATTCATAAATTTTATATAACAAACTTGGTATTTTCTCGGAAAAACTCCTGA
ATCACCCCTCGGTATTTTGTGCGTTGAGCTATCGTTAAAGCAGCCCTCGCAGAGAGCGTTCTCAAACCAAAATGGC
CGCACACGAAACAAGAGAGCGAGTGAGAGTAGGGAGAGCGTCTGTGTTGTGTGTTGAGTGTCGCCCACGCACACAG
GCGCAAAACAGTGCACACAGACGCCCGCTGGGCAAGAGAGAGTGAGAGAGAGAAACAGCGGCGCGCG
```

B. *dpp*D enhancer (719 bp)

3' of *dpp*, +29,913 to +30,629 relative to TSS of isoform D (2L:2,481,154-2,481,870)

```
AATATTTTGTTCAATTTTGTAACAGTAGAGAGAGAGCAAAATGGGTTCCACTCACCTTGTCAGCCAGTCAGTCGC
ACATCCAGTTCCTTGGCCATGTGCCCCTTTCCCCTTTGCGCTTCTCCTCCGTGTTGCCGATTCCGCCCCACACGG
AGTTAGTTTTGTCGTACACTGAAAAAAATGAACGGAAATCATGAATTTATGTTTTAGTCTGAAAGGGAGAGTTAA
AGGACACAGCATATTAATCAGGAACATAACTTCCCTTAAACTTCTTTCAACTTCTTTCAGTGCAGCTGCAGGTGT
GTGTGTTTATGGAGGACTGTGCGTCTCAAGTTTTCAACAACAAGATATAAGCCAATAAAGGAGGAACACCGGCGA
AAAGGATGAGCGGCCAGCCCAGCACACAGGGCACAAAAAGAAAGCGCAGGCAGGAGAATATACCTTAATTACGGT
TAATGGAGCGTTCGAAAAAACAAAACCGATGGCTTTATATGTGGCCCAGTGTGTGTATCATATGTTGGATCTTCG
GCCGAGTGCCACGGCGAAATAACTTAATCACATTTCGAGAGGAGACGACCGCAAAAATCTGCGAGCC
                                    Ci1
ATGTTCGTAATTTTGTATATAAATGAGATGCGGCCACCTAATGAGCCTGATTAACCAACCGGGTCCCGAGATCT
                          Ciptc: -A-----C-
                           CiKO: ---A-AA--
              Ci2                                 Ci3
TCGGTTCCTCACGGGCGGTCTCTACACCCAGCGCCGCTCCCTTGTACCTCCCC
    Ciptc: T---T----                    Ciptc: G---A---A
     CiKO: --TT-T---                     CiKO: ---A-AA--
```

C. 3xGrh + 1xCi^{ptc} (180 bp)

```
GCATGCGCTAGCAGATCTAAACCGGTTATGCGAGTCTAGACTTGGAAACCGGTTATGCGAGTCTAGACTTGGAAACCGGTTAT
GCGGCCTGGCGCGCCACTCGATGCGACCACCCAATGAGCCGCGGCCTCACGGGCTGTCTCTACGTCGACCCTTGTACATCCCC
CCCATCATGACGTC
```

D. 3xGrh alone (180 bp)

```
GCATGCGCTAGCAGATCTAAACCGGTTATGCGAGTCTAGACTTGGAAACCGGTTATGCGAGTCTAGACTTGGAAACCGGTTAT
GCGGCCTGGCGCGCCACTCGATGCGGCAACCTAATGAGCCGCGGCCTCACGGGCTGTCTCTACGTCGACCCTTGTACATCCCC
CCCATCATGACGTC
```

Sequences of enhancers used in reporter constructs or expression constructs. Ci binding sites are highlighted in yellow. (**A**) A sequence located -876 to -50 upstream of *ptc*. A *ptc* promoter fragment, including bases -758 to +130, was previously shown to drive *ptc*-like expression in

wing discs (*3*). (**B**) The *dpp*D enhancer, a 719-bp fragment downstream of *dpp*. Underlined bases represent polymorphisms relative to the "official" *D. melanogaster* genomic sequence; this fragment was isolated from w^{1118} genomic DNA. *dpp*D is a truncated version of the 800-bp "fragment 10" enhancer *(4)*. Bases altered to create *dpp*D-Ci^{ptc} and *dpp*D-Ci^{KO} are shown in red and blue, respectively. (**C** and **D**) Synthetic transgenic Ci reporters used for Figure 4. Grainyhead (Grh) sites are purple; Ci sites are red; mutated Ci sites are black. (**C**) Sequence of 3xGrh + 1xCi^{ptc}. (**D**) Sequence of the 3xGrh construct, which contains three mutated Ci sites to maintain binding site spacing relative to the previous construct.

Figure S2
Relative in vitro binding affinities of Ci binding sites regulating *ptc* and *dpp*

A

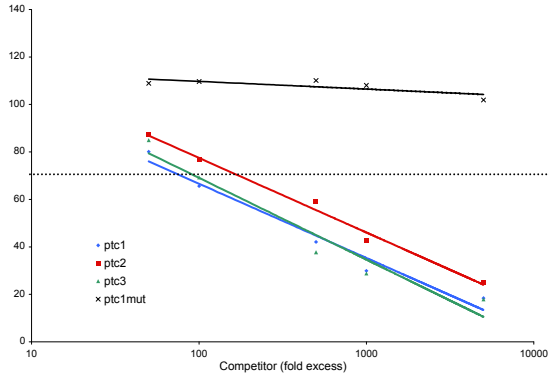

B

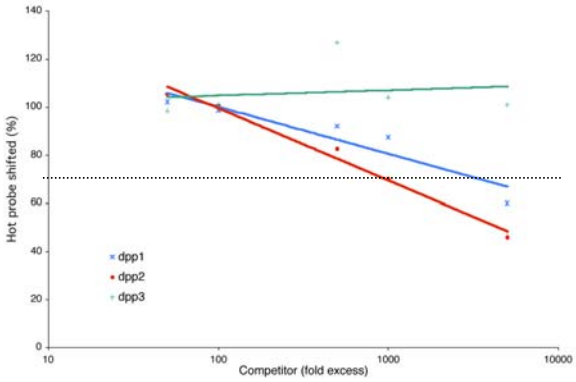

In EMSA experiments, a ^{32}P-labeled dsDNA oligonucleotide containing the ptc1 site was used as the "hot" probe. Relative in vitro affinity was determined by adding the indicated unlabeled "cold" oligonucleotides, at 50- to 50,000-fold molar excess, to in the vitro-translated Ci DNA-binding domain pre-incubated with hot ptc1 probe. The y-axis shows the amount of shifted ptc1 probe [bound/(unbound + bound)], relative to a lane lacking competitor (set at 100%). Best-fit lines were used to estimate the amount of cold competitor needed for 30% competition (dashed line); relative affinities were calculated from these ratios. (**A**) Sites ptc1-ptc3, and a mutated ptc1. (**B**) Sites dpp1-dpp3. Probe and competitor oligonucleotide sequences are provided in table S1.

Figure S3. Twelve-species alignments of Ci binding sites.

	ptc1		ptc2		ptc3	
mel	tagggGACCACCCAcatcg	1.00/1.00	gtgtgGACCACCCAaaaat	1.00/.936	gcatgGACCACCCAaagtg	1.00/.998
sim	tggggGACCACCCAcatcg	1.00/1.00	gtgtgGACCACCCAaaaat	1.00/.936	gcacgGACCACCCAaagtg	1.00/.998
sec	tggggGACCACCCAcatcg	1.00/1.00	gtgtgGACCACCCAaaaat	1.00/.936	gcacgGACCACCCAaagtg	1.00/.998
yak	gtgggGACCACCCAcaacg	1.00/1.00	gtgtgGACCACCCAaaaat	1.00/.936	gcacgGACCACCCAaagtg	1.00/.998
ere	tggggGACCACCCAcaacg	1.00/1.00	gtgggGACCACCCAaaaat	1.00/.936	gcacgGCCCACCCAaagtg	.915/.921
ana	acggaGACCACCCAcaacg	1.00/1.00	ccgggGACCACCCAaaaat	1.00/.936	tcgaaGACCACCCAaaagc	1.00/.934
pse	gctacGACCACCCAcaacg	1.00/1.00	tagcaGACCACCCAaaaat	1.00/.936	gccacGACCACCCAaaagg	1.00/.998
per	gctgcGACCACCCAcaacg	1.00/1.00	tagcaGACCACCCAaaata	1.00/.934	gccacGACCACCCAaaagg	1.00/.998
wil	ccgagGACCACCCAcaatg	1.00/1.00	tggtgGACCACCCAaatat	1.00/.936	gtttgGACCACCCAagcga	1.00/.933
vir	ctgggGACCACCCAcaatg	1.00/1.00	gcagcGACCACCCAaataa	1.00/.934	gctaaGACCACACAcgact	.907/.852
moj	ccgggGACCACCCAcaatg	1.00/1.00	gcagcGACCACCCAaataa	1.00/.934	gcttaGACCACACAcgaat	.907/.852
gri	ccgggGACCACCCAcaatg	1.00/1.00	gcagcGACCACCCAaataa	1.00/.934	ctttgGACCACACAcgact	.907/.852

	dpp1		dpp2		dpp3[a]	
mel	gatgcGGCCACCTAatgag	.812/.826	gtagaGACCGCCCGtgagg	.801/.803	ccttgTACCTCCCCcccat	.687/.651
sim	gatgcGGCCACCTAatgag	.812/.826	ggagaGACCGCCCGcgagg	.801/.818	ggtctCTCCTCCCAgcgcc	.708/.653
sec	gatgcGGCCACCTAatgag	.812/.826	ggagaGACCGCCCGcgagg	.801/.818	ggtctCTCCTCCCAgcgcc	.708/.653
yak	gatgcGGCCACCTAatgag	.812/.826	ggagaGACCGCCCGtgagg	.801/.803	tccccCTCCACCCTcctct	.680/.645
ere	gatgcGGCCACCTAatgag	.812/.826	ggagaGACCGCCCGtgagg	.801/.803	aacacCGCAACCCAttctt	.665/.616
ana	gatgcGGCCACCTAatgag	.812/.826	cagcgGACCGCCCGtgagg	.801/.803	aacttGACCAAAAAacaaa	.672/.633
pse	gatgcGGCCACCTAatgag	.812/.826	cgtcgGACCGCCCGtgtgg	.801/.803	ggcgcGAGCACCGCagatc	.661/.625
per	gatgcGGCCACCTAatgag	.812/.826	cgtcgGACCGCCCGtgtgg	.801/.803	ggcgcGAGCACCGCagatc	.661/.625
wil	gctgcGGCCACCTAatgag	.812/.826	ttagcGACCGCCTCagaga	.699/.658[b]	tgattAACCATCCAgccaa	.751/.692[b]
vir	tgagcGGCCACCTAatgag	.812/.826	ttgtcGACCGCCCGagtag	.801/.817	aatgcGCCTCTCTctctc	.618/.587
moj	tgagaGGCCACCTAatgag	.812/.826	ttgtcGACCGCCCGcgtta	.801/.753	tgaaaCACCGCTAaattgt	.590/.561
gri	tgagcGGCCACCTAatgag	.812/.826	ttgtcGACCGCCCGagtcg	.801/.817	agatgCAACACCGActcgg	.655/.685

Drosophila genomic sequences were obtained from the UCSC Genome Browser (April 2006 assembly): *mel, D. melanogaster*; *sim, D. simulans*; *sec, D. sechellia*; *yak, D. yakuba*; *ere, D. erecta*; *ana, D. ananasae*; *pse, D. pseudoobscura*; *per, D. persimilis*; *wil, D. willistoni*; *vir, D. virilis*; *moj, D. mojavensis*; *gri, D. grimshawi*. 9-bp core Ci binding sequences are in bold type; mismatches to the optimal GACCACCCA consensus are in red; flanking bases are in gray. Matrix similarity scores, shown to the right of each sequence, were calculated by the Genomatix method (*5*; the first number is calculated using positions 1-9 of a nucleotide distribution matrix derived from in vitro Ci binding data, while the second number includes data from positions 10 and 13, which make minor contributions to binding *(6)*.

[a]The rapidly-evolving dpp3 site was not easily alignable in most cases. For each species, the dpp3 site shown here represents the sequence with the highest matrix similarity score (excluding site dpp2) located between site dpp1 and the nearest downstream block of highly conserved sequence.

[b]Note that *D. willistoni*, the species with the weakest dpp2 site, has the strongest dpp3 site.

Figure S4. Improving the affinity of Ci sites in the *dpp*D enhancer causes misinterpretation of Hh gradients and lethal developmental defects.

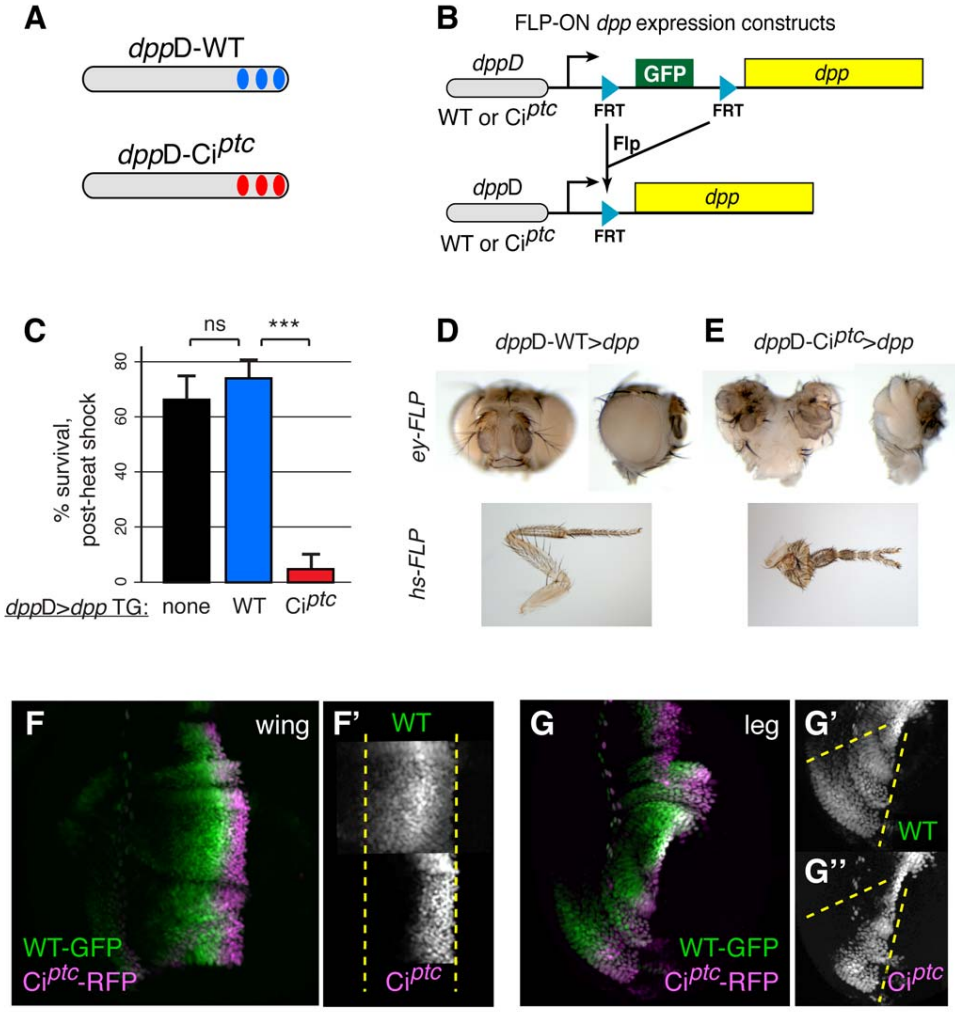

(**A**) Diagram of wild-type *dpp*D and *dpp*D-Ci^{ptc}, which contains high-affinity Ci sites (red) taken from the *ptc* enhancer. (**B**) Scheme for clonal expression of *dpp*, driven by *dpp*D-WT or *dpp*D-Ci^{ptc}. (**C**) Flies with *dpp*D-WT>*dpp* clones survive heat shock as well as controls (*P*=0.14), whereas *dpp*D-Ci^{ptc}>*dpp* clones die under the same conditions (***P=0.0005). Error bars show ± s.d. (n=3 trials, with at least 64 embryos per genotype in each trial). To calculate *P*-values, we used the arcsine transformation to normalize the data (*8*), followed by one-way Model I ANOVA (P = 1.1x10^{-5}, F-test). We made follow-up orthogonal comparisons of the sample means to the control using t-tests, as described in (*8*). (**D** and **E**) Heads and legs of pharate animals bearing *dpp*D-WT>*dpp* clones (D) or *dpp*D-Ci^{ptc}>*dpp* clones (E) induced in early larval stages. (**F** and **G**) Expression patterns of *dpp*D-WT-GFP (green) and *dpp*D-Ci^{ptc}-RFP (magenta) reporters in double-transgenic imaginal discs.

Figure S5. Overgrowth and patterning defects in imaginal discs of *dpp*D-Ci^{ptc}>*dpp* transgenic larvae.

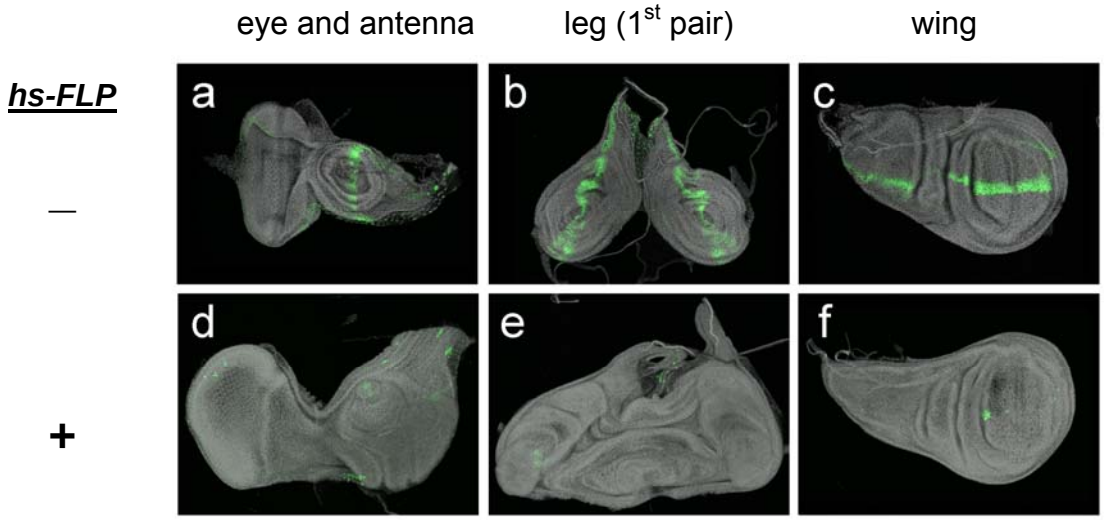

Green indicates GFP fluorescence; DAPI nuclear staining is shown in gray. Imaginal discs from late third-instar *dpp*D-Ci^{ptc}>GFP-stop>*dpp* transgenic larvae were subjected to a 1-hour 37°C heat shock during the second larval instar. (**A** to **C**) Imaginal discs in transgenic larvae without the *hs-FLP* transgene. (**D** to **F**) Imaginal discs in transgenic larvae containing one copy of *hs-FLP* and subjected to the same heat shock regime. *dpp*D-Ci^{ptc}>*dpp* did not cause defects in wing development (F), consistent with reports that the wing is less sensitive to *dpp* dose than other imaginal discs *(5, 7)*.

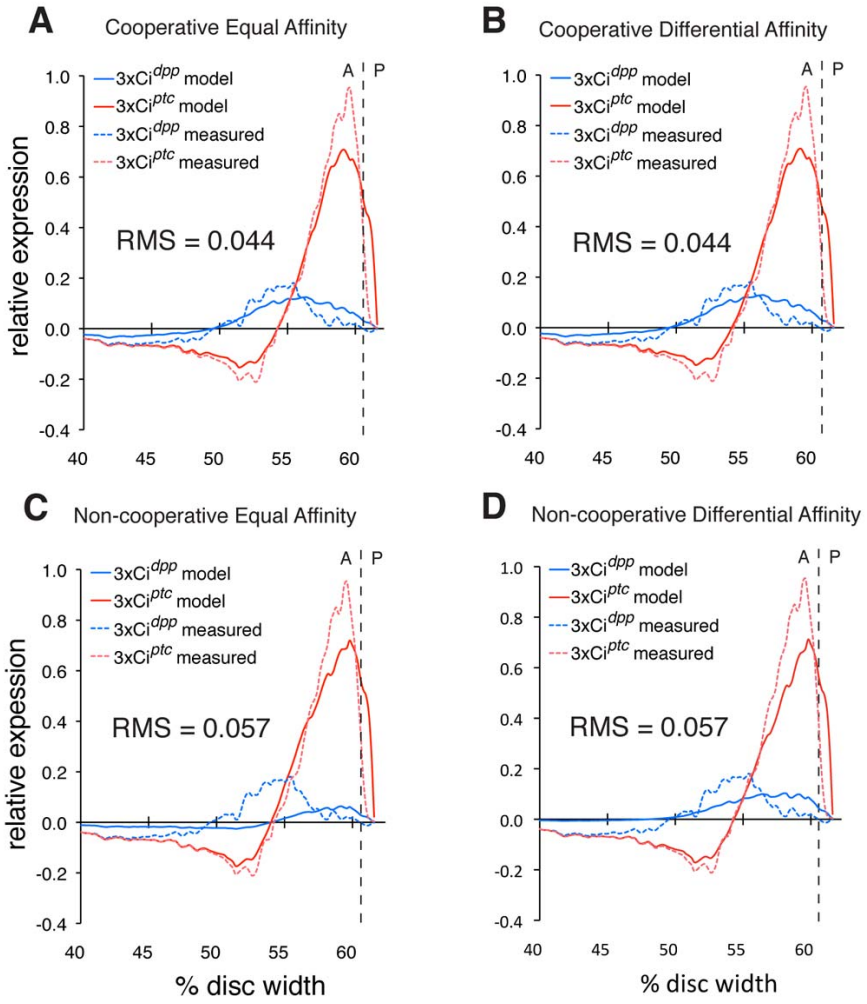

Figure S6. Best fits of four general classes of biophysical models to high-affinity ($3xCi^{ptc}$) and low-affinity ($3xCi^{wt}$) data.

Graphs show measured (dashed lines) and modeled (solid lines) relative *dpp* expression (actual expression minus basal expression, x-axis) along the Hh gradient in the wing disc (y-axis) for 3-site high-affinity (red) and 3-site low-affinity (blue) enhancers. Relative expression above the x-axis indicates activation, and values below the x-axis indicate repression. Black circles indicate the gradient position at which the models predict a switch from activation to repression. (**A** and **B**) Cooperative equal affinity and cooperative differential affinity models fit measured transgenic reporter data equally well quantitatively (RMS), and both models qualitatively captured the switch from activation to repression (black circles). (**C**) Non-cooperative equal affinity model failed to accurately capture the switch from activation to repression in the low-affinity $3xCi^{wt}$ data. (**D**) Non-cooperative differential affinity model quantitatively fit less well than cooperative models, but accurately captured regions of activation and repression. Panel D is also shown in Figure 3C.

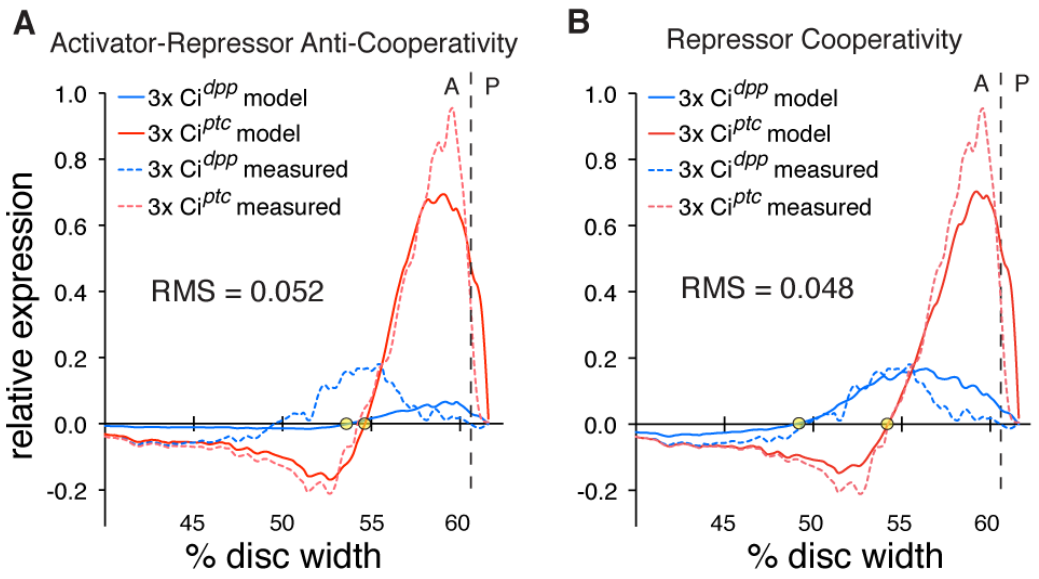

Figure S7. Best-fit equal-affinity models of individual cooperative mechanisms.

(**A**) Activator-repressor anti-cooperativity failed to accurately model the switch from activation to repression under the three-site, low affinity (3x Ci^{dpp}) enhancer. (**B**) Repressor cooperativity alone could accurately model the three-site low-affinity (3x Ci^{dpp}) and high-affinity (3x Ci^{ptc}) data quantitatively and qualitatively. Panel B is also shown in Figure 3B. See the legend for fig. S6 for a detailed description of graph axes.

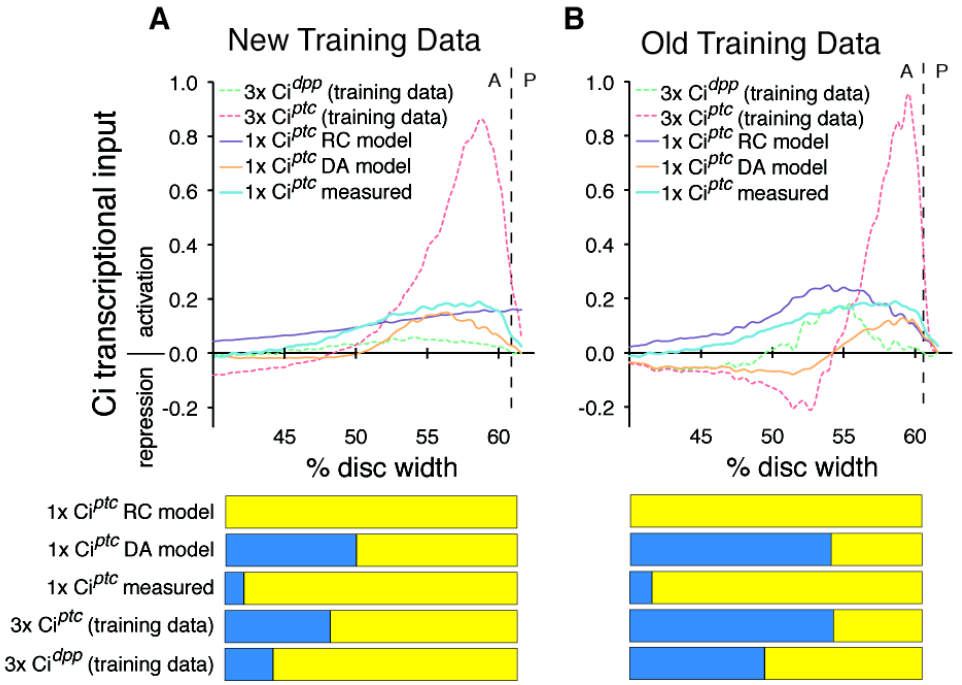

Figure S8. Prediction of single high-affinity site expression by repressor cooperativity and differential affinity models trained on new or old data.

Models make the same qualitative predictions about the location of zones of activation and repression, regardless of which data is used for model training. (**A**) Repressor cooperativity (RC) and differential affinity (DA) models retrained on the new 3xCi^{dpp} and 3xCi^{ptc} reporter gene data obtained from enhancers containing three Grainyhead sites. (**B**) Repressor cooperativity and differential affinity models trained on the original data without Grainyhead sites (this graph is also shown in Fig. 4A). These models were used to generate predictions of relative 1xCi^{ptc} expression (enhancer minus basal expression, y-axis, positive values indicate activation, negative values indicate repression) across the Hh gradient (x-axis). The repressor cooperativity model correctly predicts the main qualitative features of the 1xCi^{ptc}, whereas the differential affinity model incorrectly predicted a restricted zone of activation. Below each graph, bars indicating zones of activation (yellow) and repression (blue) across the Hh gradient show that the qualitative features of panels (A) and (B) are similar.

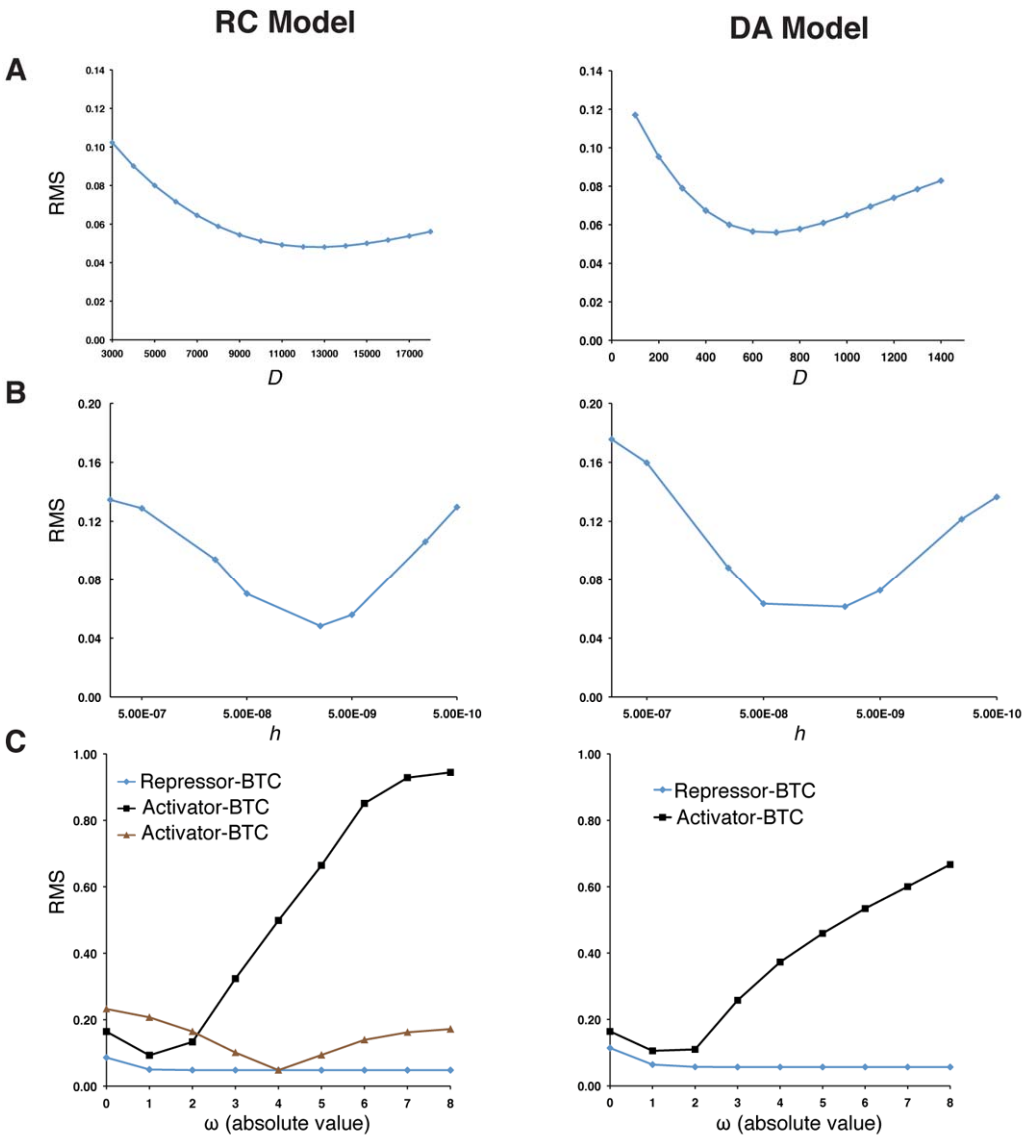

Figure S9. Repressor cooperativity and differential affinity model sensitivity to parameter changes.

Individual parameters were varied while holding the other parameters fixed at the best-fit values in table S3. (**A**) Root mean square (RMS) of the model fit as a function of gradient steepness (*D*). Lower *D* indicates a steeper gradient. (**B**) Model fit as a function of *h*, the parameter which controls total Ci concentration. (**C**) Model fit as a function of changes in cooperativity parameters (ω). Absolute values of ω are shown; the true values of repressor-repressor and activator-BTC parameters are negative (indicating favorable interactions) whereas the repressor-BTC parameter is positive.

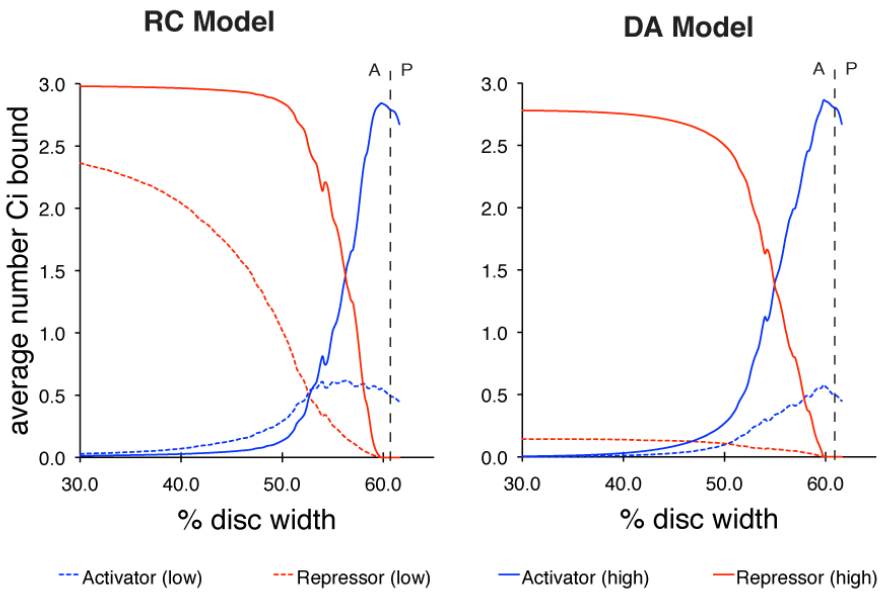

Figure S10. Repressor and activator occupancy of high- and low-affinity enhancers.

Occupancy of repressor and activator forms of Ci at three binding sites was simulated using the best-fit repressor cooperativity (RC) and differential affinity (DA) models shown in table S3. In both models, the high-affinity enhancer operates near saturation whereas the low-affinity enhancer is unsaturated.

Table S1. Sequences of EMSA oligonucleotides.

ptc1	ttgggtagggGACCACCCAcatcgcttgg
ptc1mut	ttgggtagggGA**tt**ACCCAcatcgcttgg
ptc2	ctgcagtgtgGACCACCCAaaaataaatt
ptc3	tttttgcatgGACCACCCAaagtgccttg
dpp1	aatgagatgcGGCCACCTAatgagcctga
dpp2	tgggtgtagaGACCGCCCGtgaggaaccg
dpp3	cgctcccttgTACCTCCCCcccatcatca

The top strand of each dsDNA oligonuceotide is shown.

Table S2. Parameters included in the model.

Parameter	Equal affinity model	Differential affinity model	Fit or Fixed
K_{wt}	yes	no	fit
K_{ptc}	yes	no	fixed
$K_{wt\text{-}activator}$	no	yes	fit
$K_{wt\text{-}repressor}$	no	yes	fit
$K_{ptc\text{-}activator}$	no	yes	fixed
$K_{ptc\text{-}repressor}$	no	yes	fit
$\omega(Ci_{ACT}\text{-}Ci_{ACT})$	yes	yes	fit
$\omega(Ci_{ACT}\text{-}Ci_{REP})$	yes	yes	fit
$\omega(Ci_{REP}\text{-}Ci_{REP})$	yes	yes	fit
$\omega(Ci_{ACT}\text{-BTC})$	yes	yes	fit
$\omega(Ci_{REP}\text{-BTC})$	yes	yes	fit
h	yes	yes	fit
D	yes	yes	fit

Table S3. Best-fit parameter values of four general models. The parameter values correspond to the four models shown in fig. S6.

Parameter	Cooperative Equal Affinity	Cooperative Differential Affinity	Non-Cooperative Equal Affinity	Non-Cooperative Differential Affinity
K_{wt} (low-affinity)	4.8×10^{5}	n/a	1.3×10^{6}	n/a
K_{ptc} (high-affinity)	5.0×10^{8}	n/a	5×10^{8}	n/a
$K_{wt\text{-}activator}$ (low-affinity)	n/a	4.6×10^{6}	n/a	1.1×10^{7}
$K_{wt\text{-}repressor}$ (low-affinity)	n/a	5.9×10^{6}	n/a	3.2×10^{6}
$K_{ptc\text{-}activator}$ (high-affinity)	n/a	5.0×10^{8}	n/a	5.0×10^{8}
$K_{ptc\text{-}repressor}$ (high-affinity)	n/a	5.15×10^{8}	n/a	8.1×10^{8}
$\omega(Ci_{ACT}\text{-}Ci_{ACT})$	-0.5	0.3	0	0
$\omega(Ci_{ACT}\text{-}Ci_{REP})$	8.0	10.0	0	0
$\omega(Ci_{REP}\text{-}Ci_{REP})$	-4.3	-3.3	0	0
$\omega(Ci_{ACT}\text{-BTC})$	-1.31	-1.37	-1.41	-1.47
$\omega(Ci_{REP}\text{-BTC})$	2.46	2.5	9.2	9.9
h	3.0×10^{-7}	4.0×10^{-8}	1.6×10^{-7}	2.4×10^{-8}
D	12449	9505	422	593
RMS	0.044	0.044	0.057	0.057

Table S4. Parameters for repressive cooperativity and differential affinity models. Parameter values correspond to models shown in Fig. 3, B and C.

Parameter	RC Model	DA Model
K_{wt} (low-affinity)	1.08×10^{7}	n/a
K_{ptc} (high-affinity)	5×10^{8}	n/a
$K_{wt\text{-}activator}$ (low-affinity)	n/a	1.1×10^{7}
$K_{wt\text{-}repressor}$ (low-affinity)	n/a	3.2×10^{6}
$K_{ptc\text{-}activator}$ (high-affinity)	n/a	5.0×10^{8}
$K_{ptc\text{-}repressor}$ (high-affinity)	n/a	8.1×10^{8}
$\omega(Ci_{ACT}\text{-}Ci_{ACT})$	0	0
$\omega(Ci_{ACT}\text{-}Ci_{REP})$	0	0
$\omega(Ci_{REP}\text{-}Ci_{REP})$	-4.0	0
$\omega(Ci_{ACT}\text{-BTC})$	-1.4	-1.5
$\omega(Ci_{REP}\text{-BTC})$	6.3	9.9
h	1.77×10^{-8}	2.4×10^{-8}
D	12445	593
RMS	0.048	0.057

References

1. G.v. Dassow, E. Meir, E.M. Munro, G.M. Odell, The segment polarity network is a robust developmental module. *Nature* **406**, 188-192 (2000).
2. S. Barolo, L. A. Carver, J. W. Posakony, GFP and ß-galactosidase transformation vectors for promoter/enhancer analysis in *Drosophila*. *BioTechniques* **29**, 726-732 (2000).
3. C. Alexandre, A. Jacinto, P.W. Ingham, Transcriptional activation of hedgehog target genes in *Drosophila* is mediated directly by the cubitus interruptus protein, a member of the GLI family of zinc finger DNA-binding proteins. *Genes & Development* **10**, 2003-2013 (1996).
4. B. Müller, K. Basler, The repressor and activator forms of Cubitus interruptus control Hedgehog target genes through common generic gli-binding sites. *Development* **127**, 2999-3007 (2000).
5. S. Morimura, L. Maves, Y. Chen, F.M. Hoffmann, *decapentaplegic* overexpression affects *Drosophila* wing and leg imaginal disc development and *wingless* expression. *Developmental Biology* **177**, 136-151 (1996).
6. O. Hallikas, K. Palin, N. Sinjushina, R. Rautiainen, J. Partanen, E. Ukkonen, J. Taipale, Genome-wide prediction of mammalian enhancers based on analysis of transcription-factor binding affinity. *Cell* **124**, 47-59 (2006).
7. M. Zecca, K. Basler, G. Struhl, Sequential organizing activities of engrailed, hedgehog and decapentaplegic in the Drosophila wing. *Development* **121**, 2265-2278 (1995).
8. R.R. Sokal, F.J. Rohlf, *Biometry* (Freeman, New York, ed. 3, 1995).